J. Fluid Mech. (1978), *vol.* 85, *part* 4, *pp.* 655–672
Printed in Great Britain

Bubble plumes in stratified environments

By TREVOR J. McDOUGALL
Department of Applied Mathematics and Theoretical Physics, University of Cambridge

(Received 20 February 1976 and in revised form 15 September 1977)

This paper is concerned with the behaviour of buoyant plumes driven by a source of bubbles. It is shown experimentally that, when a bubble plume rises through a stratified environment, fluid can be transported vertically for some distance and then some of this fluid can leave the plume and spread out horizontally at its own density level. A simple plume model which regards the plume as a single entity is discussed in order to make a first assessment of the effects of gas expansion and bubble slip velocity in this stratified case. However, the experiments reveal a more complicated plume structure in which the bubbles remain in the centre part of the plume, and only the outer part of the plume spreads out into the environment at certain levels. On the basis of these observations a double-plume model is proposed which regards the plume as being composed of two parts: an inner circular plume (which contains all the bubbles of gas) and an outer annular plume.

1. Introduction

Buoyant plumes driven by a source of gas bubbles have found a number of uses over the years. Bubble breakwaters operate because of the surface jet which the plume produces (Taylor 1955) and have been used with varying degrees of success (Bulson 1968). Bubble plumes have also been used to prevent parts of the surface of a river or lake from freezing over (Baines 1961). Oil slicks on water surfaces can be contained by bubble plumes (Jones 1972). Protection from underwater-explosion damage is another application. Bubble plumes have also been used to keep swimming areas free from slow-moving objects such as sea nettles (Marks & Cargo 1974).

The current interest in bubble plumes arose in connexion with the consequences of an underwater oil-well blow-out. Characteristically a lot of gas is emitted along with the oil, and the plume which develops is mainly due to the presence of the bubbles which are formed from this gas (Topham 1974). Oil is very harmful to marine life and is very difficult to clean up in the ocean (Hoult 1969). The extent of the damage which results from an oil-well blow-out is strongly dependent on whether all the oil rises straight to the surface or whether some of it spreads out horizontally at some intermediate depth (perhaps as an oil–water emulsion).

A bubble plume is different to a plume driven by a normal source of buoyancy, in three important respects. First, the volume flow rate of gas will increase with height because the pressure acting on the gas decreases. Second, the bubbles will rise faster than the liquid part of the plume surrounding them. Third, in a stratified environment, the bubbles will continue to rise past any height at which simple plume theory predicts that the plume as a whole would stop rising and would spread out horizontally.

The current work begins by using the horizontally integrated equations of conserva-

tion of mass, momentum and buoyancy (Morton, Taylor & Turner 1956) in an appropriate form for bubble plumes. We shall speak of an ordinary (or normal) plume as being one driven by a source of buoyancy such as heat or a concentration difference and in which the plume fluid is homogeneous in the sense that it is not composed of a fine mixture of two substances (such as liquid and gas). Morton *et al.* (1956) have found for an ordinary plume in a stratified environment that a height is reached at which the buoyancy is zero, and as the plume proceeds above this level (because of its inertia), it continues to slow down, gaining negative buoyancy. Eventually the plume stops rising altogether, finally spreading out at a height somewhat less than the maximum height reached by the plume. In the case of a bubble plume, the bubbles themselves will not of course settle out at an intermediate height and this is one of the main differences to be elucidated here. The first model for a bubble plume in stratified surroundings described in this paper has no in-built mechanism whereby the liquid part of the plume and the bubbles can separate near this intermediate height, and so this model will not give realistic results near this level. However it is instructive to go through the derivation of this model because while Ditmars & Cederwall (1974) have described the behaviour due to gas expansion and bubble slipping, the current work also includes the effects of stratification. It is easier to see how to include stratification by considering a single-plume model, so this is a helpful preliminary to formulating the more realistic double-plume model.

Experiments were carried out in a stratified environment, and as expected, these show that fluid can leave the plume and spread out horizontally, while the centre of the plume, where all the bubbles are concentrated, continues to rise. On the basis of these experimental observations, a 'double-plume' model is proposed. This model has a circular inner plume in which all the bubbles are confined, surrounded by an annular outer plume which contains only liquid. A series of conservation equations are derived for this model and are solved numerically for several values of the parameters involved.

2. First plume model

Consider a point source of gas at a depth h below the liquid surface (figure 1). Let $Q(z)$ be the steady flow rate of gas at any height z above the point source and let Q_0 be $Q(h)$, the value of Q at the surface. By assuming isothermal expansion of the gas bubbles as they rise, we find that constancy of the mass flow rate of the gas implies

$$Q(z) = Q_0 p_a/(H-z)\rho_r g, \tag{1}$$

where p_a = pressure at the surface (i.e. atmospheric pressure),
g = gravitational acceleration,
ρ_r = reference liquid density,
$H = h + p_a/\rho_r g = h + 10{\cdot}2\,\mathrm{m}$ = static pressure head at nozzle.

In the oil-well problem the gas and oil may emerge at 85 °C but the heat transfer between the sea water and the gas bubbles will soon ensure that the bubbles are at the same temperature as the water and hence isothermal expansion can be assumed. (The e-folding time for the temperature difference is about 1 s.) Also the heat supplied at the nozzle has a negligible effect on the buoyancy of the plume in comparison with the presence of the bubbles (Topham 1974).

It is convenient to assume an average vertical velocity profile given by

$$v(r,z) = v(z)\exp(-r^2/b^2),$$

where $v(r,z)$ = vertical velocity at height z and radius r, $v(z)$ = vertical velocity on centre-line at height z, b = effective radius of plume. This has some experimental support in unstratified surroundings (Kobus 1968), but in any case the exact form of the profile is not important in determining the physics of the model; the only essential assumption is that the profiles are similar at all heights.

It is usual to assume that the distribution of the density deficiency can also be represented by a Gaussian profile, but in this case with a spread λb, i.e.

$$g'(r,z) = g'(z)\exp(-r^2/\lambda^2 b^2),$$

where

$$g'(r,z) = (g/\rho_r)(\rho_0(z)-\rho(r,z))$$

and $\rho_0(z)$ = density of environment at height z.

Three differential equations can be found which describe the motion of the plume; these are obtained from (i) conservation of mass, (ii) conservation of momentum and (iii) conservation of buoyancy. We shall consider each of these in turn.

Mass conservation around a horizontal element of the plume yields

$$\frac{d}{dz}\left(\int_0^\infty v\exp\left(-\frac{r^2}{b^2}\right)2\pi r\,dr\right) = 2\pi b u_e,$$

and using the entrainment assumption $u_e = \alpha v$ (where u_e is the entrainment velocity and α is called the entrainment constant), we obtain

$$d(b^2 v)/dz = 2\alpha b v. \tag{2}$$

Momentum conservation for the same horizontal element of the plume yields

$$\frac{d}{dz}\left(\int_0^\infty \rho v^2\exp\left(-\frac{2r^2}{b^2}\right)2\pi r\,dr\right) = \int_0^\infty \rho_r g'\exp\left(-\frac{r^2}{\lambda^2 b^2}\right)2\pi r\,dr,$$

and using the Boussinesq approximation, we obtain

$$d(\tfrac{1}{2}b^2 v^2)/dz = \lambda^2 b^2 g'. \tag{3}$$

Now the conservation of buoyancy is concerned with two separate effects: first, the effect of the stratification $d\rho_0/dz$ in the environment, and second, the increase in the volume flow rate of gas with height. It is helpful to isolate these two effects by considering first an ordinary plume rising in a stratified environment. Conservation of buoyancy then yields

$$\frac{d}{dz}\left(\int_0^\infty v(r,z)\,[\rho_0(z)-\rho(r,z)]\,2\pi r\,dr\right) = \pi b^2 v\frac{d\rho_0}{dz},$$

or

$$\left[\frac{d}{dz}\left(\frac{\pi\lambda^2 b^2 v g'}{\lambda^2+1}\right)\right]_{\text{strat}} = -\pi b^2 v N^2(z), \tag{4}$$

where $N(z) = (-g\rho_r^{-1}d\rho_0/dz)^{\frac{1}{2}}$ is the local buoyancy frequency. Equation (4) can be interpreted as a relation concerning the quantity $\rho_r^{-1}d(\text{flux of weight deficiency})/dz$, and expresses the way this quantity changes owing to the effect of stratification.

Second, let us consider a bubble plume rising in unstratified surroundings. The

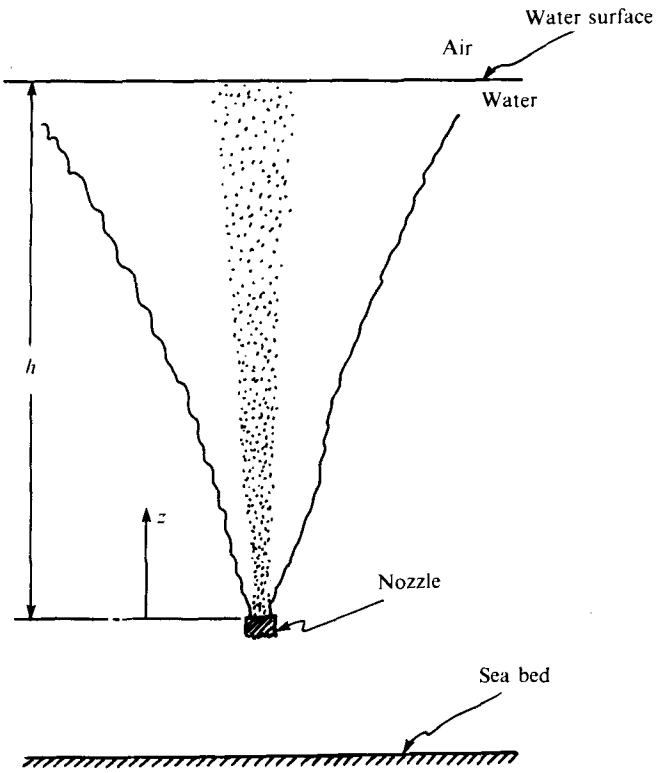

FIGURE 1. Diagram showing a 'point' source of bubbles at depth h driving a plume to the surface.

density $\rho(r, z)$ at any point is the average effective density of a small region of the gas–liquid mixture, where this average is taken over a volume containing many bubbles. $\rho_0(z)$ is now constant and the local ratio of the volume of gas to the volume of the mixture is given by $g'(r, z)/g$. The total average rise velocity of the individual bubbles is $v(r, z) + u_s$ (where u_s is the slip velocity of the bubbles with respect to the rising plume), and from this it is possible to find a relation between Q_0, v and g' by noting that at any height the actual volume flow rate of bubbles is $Q(z)$. Therefore

$$Q(z) = \frac{Q_0 p_a}{(H-z)\rho_r g} = \int_0^\infty [v(r,z)+u_s]\frac{g'(r,z)}{g} 2\pi r\, dr,$$

or

$$\lambda^2 g' b^2 = Q_0 p_a(\lambda^2+1)/(H-z)\pi\rho_r(v+u_B), \tag{5}$$

where $u_B = u_s(\lambda^2+1)$. The contribution to the quantity $\rho_r^{-1} d(\text{flux of weight deficiency})/dz$ due to the effect of gas expansion is then

$$\left[\frac{d}{dz}\left(\frac{\pi\lambda^2 b^2 v g'}{\lambda^2+1}\right)\right]_{\text{exp}} = \frac{d}{dz}\left(\frac{Q_0 p_a v}{(H-z)\rho_r(v+u_B)}\right). \tag{6}$$

Equations (4) and (6) can now be summed to obtain

$$\frac{d}{dz}\left(\frac{\pi\lambda^2 b^2 v g'}{\lambda^2+1}\right) = -\pi b^2 v N^2 + \frac{d}{dz}\left(\frac{Q_0 p_a v}{(H-z)\rho_r(v+u_B)}\right). \tag{7}$$

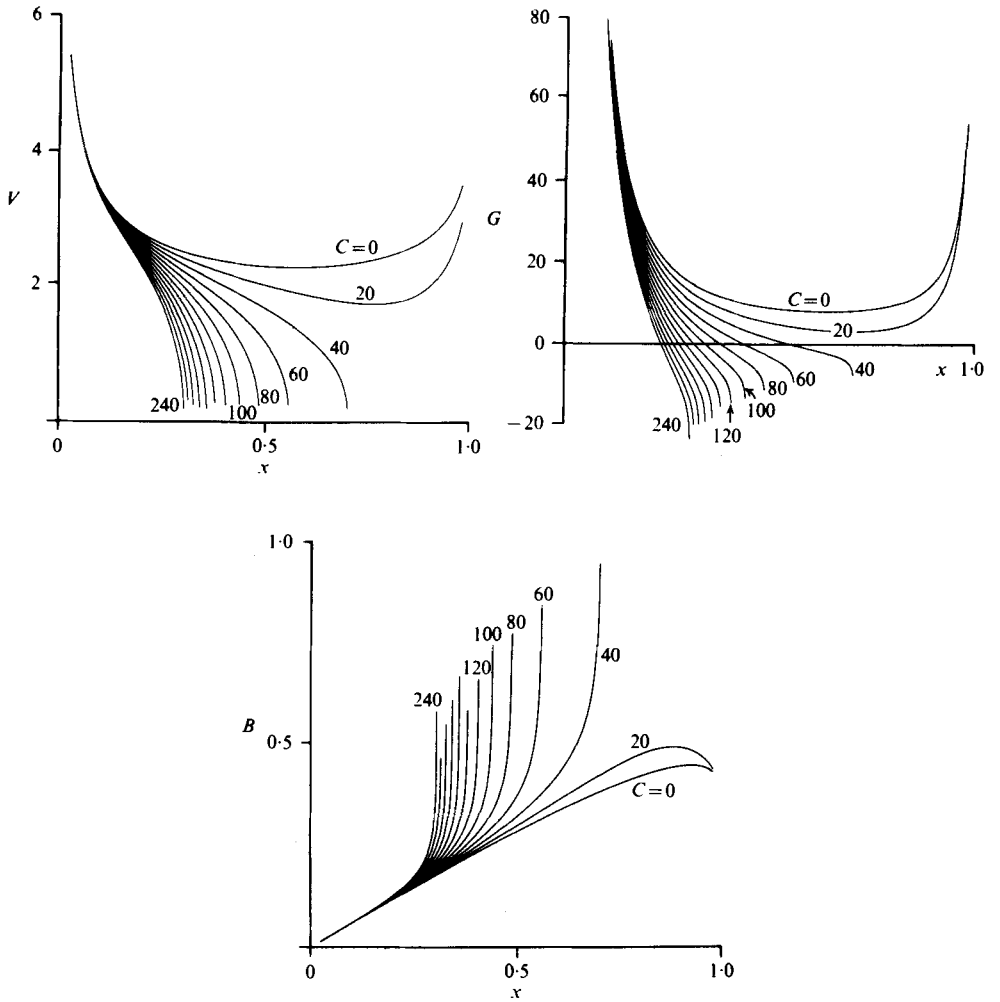

FIGURE 2. Graphs of velocity V, radius B and buoyancy G for the single-plume point-source model for a source strength M of 10 and for values of the stratification parameter C from 0 to 240.

The rise velocity of individual bubbles through a liquid is a function of their size, and as the bubbles rise and expand, it may be expected that their slip velocity will vary. However, it has been shown experimentally that, in a bubble plume such as ours, individual bubbles break up when they grow beyond a certain size and small bubbles coalesce until a stable bubble size is reached (Jones 1972). The size of the bubbles in the plume thus tends to be nearly constant and their velocity u_s relative to the moving plume may be assumed constant. This slip velocity reduces the effective buoyancy flux because the bubbles spend less time communicating their buoyancy to the plume.

Equations (2), (3) and (7), together with appropriate boundary conditions, completely describe this plume model. Non-dimensional variables are chosen as follows:

$$z = Hx, \quad b = 2\alpha HB, \quad v = u_B M^{\frac{1}{3}} V, \quad g' = (u_B^2 M^{\frac{2}{3}}/\lambda^2 H) G,$$

where $M = Q_0 p_a(\lambda^2+1)/4\pi\alpha^2\rho_r H^2 u_B^3$. If u_B is taken to be constant, M is proportional

to Q_0/H^2, which by (1) is proportional to $Q(0)/H$. Thus M simply represents the relative importance of (i) the volume flux of gas at the source and (ii) the total water depth in the non-dimensional solutions.

Upon substituting these non-dimensional variables, (2), (3) and (7) become

$$\frac{d}{dx}(B^2V) = BV, \quad \frac{d}{dx}(BV) = \frac{BG}{V}, \tag{8),(9}$$

$$\frac{d}{dx}(B^2VG) = -CB^2V + \frac{d}{dx}\left(\frac{V}{(1-x)(V+M^{-\frac{1}{3}})}\right), \tag{10}$$

where $$C(x) = N^2(\lambda^2+1)H^2/u_B^2M^{\frac{2}{3}}.$$

The solutions will thus depend on the two parameters M and C, and we shall need to find an appropriate way of initializing the integration of (8)–(10). Morton *et al.* (1956) found that at small heights an ordinary plume is not influenced very much by the stratification and so in the current situation it is considered appropriate to put $C = 0$ for the purpose of finding the initial values of B^2V and BV at small x. The initial value of B^2VG can be obtained from (5), and is $V/(1-x)(V+M^{-\frac{1}{3}})$. This value of B^2VG also satisfies (10). At $x = 0$, $B^2V^2 = B^2V = 0$ and (8) and (9) now have the power-series solution

$$B = x[0{\cdot}6 + 0{\cdot}01719M^{-\frac{1}{3}}x^{\frac{1}{3}} - 0{\cdot}002527M^{-\frac{2}{3}}x^{\frac{2}{3}} + x(-0{\cdot}04609 + 0{\cdot}000031M^{-1}) + \ldots], \tag{11}$$

$$V = x^{-\frac{1}{3}}[1{\cdot}609 - 0{\cdot}3195M^{-\frac{1}{3}}x^{\frac{1}{3}} + 0{\cdot}06693M^{-\frac{2}{3}}x^{\frac{2}{3}} + x(0{\cdot}4536 - 0{\cdot}0105M^{-1}) + \ldots]. \tag{12}$$

Equations (8)–(10) were solved numerically by a Runge–Kutta method with initial conditions obtained from the above power-series solutions for a starting value of $x = 0{\cdot}025$. In each case the stratification was assumed to be linear, implying that the value of C is independent of depth, but this of course is not necessary and solutions can readily be obtained if C is specified as a function of x.

Figure 2 shows the effect of varying the stratification parameter C while keeping the source strength parameter M constant and equal to 10. As may be expected, the model predicts that the final height of the plume is less for greater stratification. For plumes which do not spread out before reaching high values of x, the effects of bubble expansion can be seen (e.g. the curves for $C = 0$ and $C = 20$ in figure 2). The buoyancy G and velocity V now increase dramatically owing to the large decrease in static pressure and the consequent increase in gas volume.

A similar model to the above has been developed for a two-dimensional bubble plume which is driven by a line source of gas; the results show the same qualitative features as the point-source solutions.

3. Double-plume model

3.1. *Experimental observations*

Experiments were carried out in a Perspex tank of square horizontal cross-section ($0{\cdot}6 \times 0{\cdot}6$ m) which was normally filled to a height of approximately 1·3 m with linearly stratified salt solution. Air was introduced into the tank through a nozzle in the tank floor. In order to simulate a large-scale plume as well as possible it is desirable to make

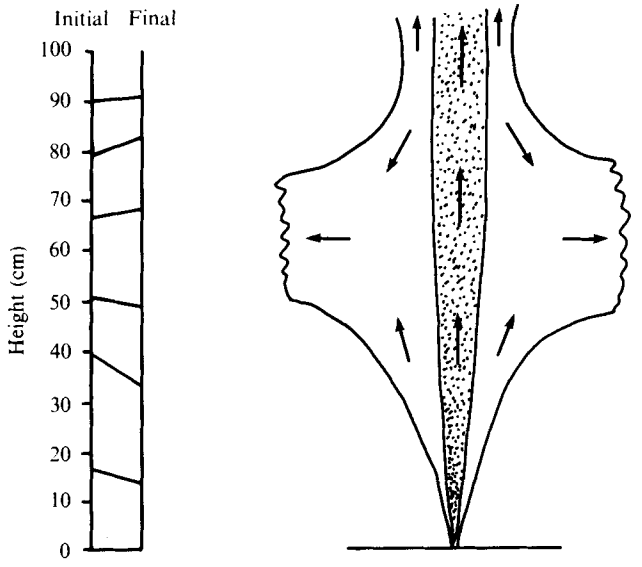

FIGURE 3. Diagram of the shadowgraph during an experiment with $h = 1{\cdot}3$ m, $Q_0 = 27$ c.c./s and $N^2 = 0{\cdot}41$ s^{-2} (if we take $\alpha = 0{\cdot}1$, $\lambda = 0{\cdot}3$ and $u_s = 0{\cdot}28$ m/s, this leads to $M = 0{\cdot}007$ and $C = 11000$). The positions of six buoyancy bottles (which mark layers of constant density) are shown before and after the experiment. Lines are drawn between the two positions of each bottle. The model gave the first spreading-out level at $x = 0{\cdot}039$, i.e. $z = 45$ cm, whereas it can be seen in fact to occur at $z \approx 60$ cm.

the bubble size small. This makes the 'average plume density' a meaningful quantity, thereby ensuring plume-like behaviour and not simply that of a rapid succession of individual bubbles. Also, small bubbles have a low slip velocity and hence M ($\propto u_s^{-3}$) is increased to a value closer to what we envisage for the oil-well blow-out problem in the ocean. In an effort to reduce the bubble size, several additives were tried, including methylated spirits and detergent, but the most effective was octanoic acid, which was used at a concentration of 30 p.p.m. Various types of nozzle were also tried and in the most successful arrangement the air was blown through a small piece of foam. The bubbles which were obtained were estimated to have a diameter of approximately 1·25 mm.

In order to find out where the plume was entraining and where it was losing fluid, observations were made of the movement of dye which marked layers of constant density. These dye layers were put in by means of a syringe which fitted into a non-return valve mechanism, so that dye could be mixed with the fluid which was going into the tank, just before it actually entered the tank. The layers of dye were about 1 cm thick and were put in at a vertical spacing of approximately 10 cm. Another way of marking layers of constant density was developed by constructing small coloured bottles of specified density, which were allowed to float freely in the tank. The time history of the separation between two adjacent density levels gives an indication of whether the plume has had a net entraining effect or a net 'detraining' effect between these levels.

With the air flow turned on at the desired rate, the positions of the layers were noted at various times. These results show that, during the course of an experiment for which

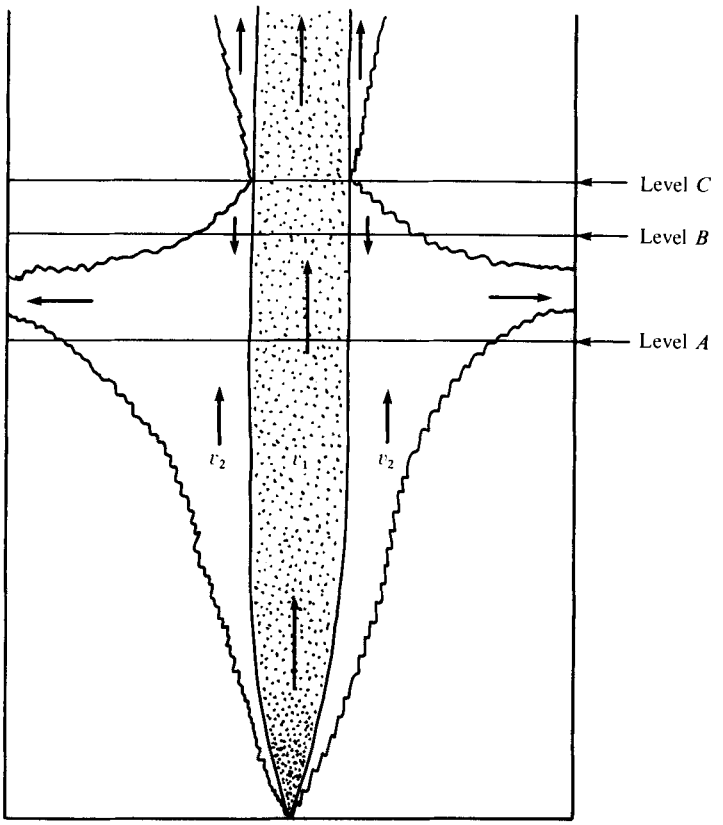

FIGURE 5. Diagram of the spreading-out stage of the double-plume model. Level A is where the outer plume has slowed to a very small velocity, level B is where the upward and downward mass fluxes sum to zero and level C is where the double-plume model starts again.

the first plume model predicted that the plume would spread out at some intermediate level, the layers near the bottom moved closer together, while at some higher levels the layers moved further apart. This indicated that the net effect of the plume at the lower level had been to entrain fluid, while at the higher levels the plume had been losing fluid to the environment. Experiments using a shadowgraph to observe the motion showed that fluid was indeed leaving the plume at these upper levels, and spreading out horizontally. Direct observations of the experiments showed that the bubbles rose to the surface in a narrow region, which we shall call the inner plume, and that the velocity of this inner plume did not vary very much, even at levels where the shadowgraph showed the outer plume to be spreading out. The radius of the inner plume was typically one-third of the radius of the outer plume.

At a small distance above the spreading-out region, a layer was sometimes observed which did not move either up or down during the course of an experiment. This implies that there must have been an annular region around the inner plume which was descending in such a way that the two mass flow rates past this level were exactly balanced. This behaviour could also be seen on a shadowgraph.

An example of the movements of these constant-density levels can be seen in

figure 3. When experiments are performed with a strongly stratified environment, the plume is seen to lose fluid to the environment at many different levels (see the shadowgraphs in figure 4, plate 1).

3.2. *The model*

3.2.1. *The model equations.* The observations described above led to the proposal of a 'double-plume' structure in which all the bubbles are confined to an inner plume which continues to rise all the way to the surface, while the outer plume contains only liquid. Initially the outer plume rises at some fraction of the velocity of the inside plume, but since it is denser than its surroundings, it will slow down and eventually stop rising and start to spread out horizontally, as shown in figure 5. The downflow at B in this figure may be thought of as analogous to the motion of an ordinary plume after it has reached its maximum height. Level A is a height at which the outside plume has slowed down to a very small upward velocity and its outside radius has begun to increase very rapidly. Level B is the level described above, where the mass fluxes of the inner and outer plumes sum to zero. Level C is where the double-plume structure starts again; the inner plume now has large mass and momentum fluxes and the outer plume is assumed to start with zero mass and momentum fluxes. Although the outer plume was never observed to neck down as much as is shown at this level, this proved to be a necessary expedient in order to restart the solution.

In order to obtain some equations which will describe the motion of this double-plume structure, it is necessary to make some realistic assumptions about the rate of entrainment of fluid into and out of each plume. The usual entrainment assumption for an ordinary plume ($u_e = \alpha v$) implies that there is only one velocity scale in the problem at each height; this is consistent with the solutions for an unstratified environment and has been shown to give good agreement between theory and experiment for ordinary plumes rising through a stratified environment (Morton *et al.* 1956).

The velocity of the outer plume will be representative of the velocity difference in the shear layer between the outer plume and the environment. It seems plausible to extend the widely used entrainment assumption to this situation and to assume that the velocity of entrainment of fluid from the environment into the outer plume is proportional to the velocity of this outer plume. Similarly, the entrainment of fluid into the inner plume from the outer plume will be proportional to the velocity difference between the plumes. Also, the outer plume, because of its own turbulence, will entrain fluid from the inner plume, and this entrainment velocity will scale with a typical turbulent velocity in the outer plume. Turner (1963) has used this assumption to model the loss of fluid from a rising turbulent thermal, owing to environmental turbulence. Morton (1962) has pointed out that the relevant velocity scale on which to base this entrainment is the velocity of the outer plume.

In the absence of any experimental observations, top-hat profiles of velocity and buoyancy will be assumed. This will simplify the derivation but does not restrict the generality of the model provided that the profiles remain similar at all heights. The entrainment constants for each of the three entrainment processes are not assumed to be equal, but are α for the entrainment of environment fluid into the outer plume, α_β for the entrainment of fluid into the inner plume and α_γ for the rate of transfer of liquid from the inner plume into the outer plume.

The conservation of mass for the inner (subscript 1) plume then gives

$$d(r_1^2 v_1)/dz = 2r_1\alpha_\beta(v_1 - v_2) - 2r_1\alpha_\gamma|v_2| \tag{13}$$

and similarly for the outer (subscript 2) plume

$$d[(r_2^2 - r_1^2)v_2]/dz = -2r_1\alpha_\beta(v_1 - v_2) + 2r_1\alpha_\gamma|v_2| + 2r_2\alpha|v_2|. \tag{14}$$

The normal equations for a single plume assume that constant-pressure surfaces remain horizontal, and this implies that the buoyant force on the plume is simply $g(\rho_0 - \rho)$ multiplied by its area. This will be a good approximation when the sides of the plume are close to the vertical. Making the same assumption for this model means that the buoyant force on each plume can be found by referring the plume's density to the density of the environment. The conservation equations of vertical momentum then become

$$d(r_1^2 v_1^2)/dz = r_1^2 g_1' + 2r_1\alpha_\beta v_2(v_1 - v_2) - 2r_1\alpha_\gamma v_1|v_2|, \tag{15}$$

$$d[(r_2^2 - r_1^2)v_2^2]/dz = -(r_2^2 - r_1^2)g_2' - 2r_1\alpha_\beta v_2(v_1 - v_2) + 2r_1\alpha_\gamma v_1|v_2|, \tag{16}$$

where

$$g_1' = \frac{g}{\rho_r}(\rho_0 - \rho_1), \quad g_2' = \frac{g}{\rho_r}(\rho_2 - \rho_0).$$

This definition of g_2' has been chosen to keep it positive. Further discussion on the body forces in this model is given in appendix B.

In the derivation of the equations for the conservation of buoyancy, it must be remembered that the fluid which is entrained by the outer plume from the inner plume has a density different to the average density of the inner plume because the bubbles are not entrained but remain in the inner plume. Let ρ_{1l} be the density of the liquid part of the inner plume and ρ_1 be the overall density of the inner plume. At any height, conservation of bubble volume requires that

$$Q(z) = Q_0 p_a/(H - z)\rho_r g = \pi r_1^2(v + u_s)A(z), \tag{17}$$

where $A(z)$ is the local volume fraction which is occupied by the air. Consider a small volume in the inner plume which contains many bubbles. The overall density of this volume will be given by

$$\rho_1 = (1 - A)\rho_{1l} + A\rho_{\mathrm{air}}$$

and since $\rho_{\mathrm{air}}/\rho_r \approx 10^{-3}$ this equation approximates to

$$g_1' = g_{1l}' + gA, \tag{18}$$

where $g_{1l}' = g/\rho_r^{-1}(\rho_0 - \rho_{1l})$. The equations of conservation of buoyancy can now be obtained by applying the same arguments as were used to derive (7):

$$\frac{d}{dz}(r_1^2 v_1 g_1') = r_1^2 v_1 \frac{g}{\rho_r}\frac{d\rho_0}{dz} - 2r_1\alpha_\beta(v_1 - v_2)g_2' - 2r_1\alpha_\gamma|v_2|g_{1l}' + \frac{d}{dz}(r_1^2 g v_1 A), \tag{19}$$

$$-\frac{d}{dz}[(r_2^2 - r_1^2)v_2 g_2'] = (r_2^2 - r_1^2)v_2\frac{g}{\rho_r}\frac{d\rho_0}{dz} + 2r_1\alpha_\beta(v_1 - v_2)g_2' + 2r_1\alpha_\gamma|v_2|g_{1l}'. \tag{20}$$

Equations (13)–(20) describe the model. They may be non-dimensionalized by putting

$$r_1 = 2\alpha H R_1, \quad r_2 = 2\alpha H R_2, \quad v_1 = u_s M^{\frac{1}{3}} V_1, \quad v_2 = u_s M^{\frac{1}{3}} V_2,$$

$$g_1' = \frac{u_s^2 M^{\frac{2}{3}}}{H} G_1, \quad g_2' = \frac{u_s^2 M^{\frac{2}{3}}}{H} G_2, \quad S^2 = R_2^2 - R_1^2, \quad z = Hx,$$

$$\beta = \frac{\alpha_\beta}{\alpha}, \quad \gamma = \frac{\alpha_\gamma}{\alpha}, \quad G_{1L} = G_1 - \frac{1}{(1 - x)(V_1 + M^{-\frac{1}{3}})R_1^2},$$

where $$M = \frac{Q_0 p_a}{4\pi\alpha^2\rho_r H^2 u_s^3}, \quad C(x) = \frac{H^2N^2}{u_s^2 M^{\frac{2}{3}}}.$$

The equations then become

$$d(R_1^2V_1)/dx = \beta R_1(V_1 - V_2) - \gamma R_1|V_2|, \tag{21}$$

$$d(S^2V_2)/dx = -\beta R_1(V_1 - V_2) + \gamma R_1|V_2| + R_2|V_2|, \tag{22}$$

$$d(R_1^2V_1^2)/dx = R_1^2G_1 + \beta R_1V_2(V_1 - V_2) - \gamma R_1V_1|V_2|, \tag{23}$$

$$d(S^2V_2^2)/dx = -S^2G_2 - \beta R_1V_2(V_1 - V_2) + \gamma R_1V_1|V_2|, \tag{24}$$

$$\frac{d}{dx}(R_1^2V_1G_1) = -R_1^2V_1C - \beta R_1G_2(V_1 - V_2) - \gamma R_1|V_2|\,G_{1L} + \frac{d}{dx}\left(\frac{V_1}{(1-x)(V_1 + M^{-\frac{1}{3}})}\right) \tag{25}$$

and $$-d(S^2V_2G_2)/dx = -S^2V_2C + \beta R_1G_2(V_1 - V_2) + \gamma R_1|V_2|\,G_{1L}. \tag{26}$$

With suitable starting conditions the above equations can be solved by a Runge–Kutta procedure.

3.2.2. *Starting conditions.* At the small starting value of x, the stratification of the environment will have had a negligible effect so the buoyancy of the inner plume will be entirely due to the bubbles, and therefore $G_{1L} = 0$, i.e.

$$G_1 = 1/(1-x)(V_1 + M^{-\frac{1}{3}})R_1^2. \tag{27}$$

At this level G_2 is very small and so we assume that it is zero. V_2 is positive here and so the differential equations to be solved by power series reduce to

$$d(R_1^2V_1)/dx = \beta R_1V_1 - (\gamma + \beta)R_1V_2, \tag{28}$$

$$d(S^2V_2)/dx = -\beta R_1V_1 + (\gamma + \beta)R_1V_2 + R_2V_2, \tag{29}$$

$$d(R_1^2V_1^2)/dx = 1/(1-x)(V_1 + M^{-\frac{1}{3}}) - (\gamma - \beta)R_1V_1V_2 - \beta R_1V_2^2, \tag{30}$$

$$d(S^2V_2^2)/dx = \beta R_1V_2^2 + (\gamma - \beta)R_1V_1V_2. \tag{31}$$

By analogy with the form of the power-series solution of the single-plume model [(11) and (12)], we choose the following series:

$$\begin{aligned} R_1 &= x(r_1 + x^{\frac{1}{3}}r_2 + \ldots), \\ V_1 &= x^{-\frac{1}{3}}(v_1 + x^{\frac{1}{3}}v_2 + \ldots), \\ S &= x(b_1 + x^{\frac{1}{3}}b_2 + \ldots), \\ V_2 &= x^{-\frac{1}{3}}(d_1 + x^{\frac{1}{3}}d_2 + \ldots). \end{aligned}$$

The method of solution for these coefficients is given in appendix A.

3.2.3. *Numerical treatment of the spreading out.* The numerical method will proceed as far as level A on figure 5, where the velocity V_2 will be very small and the radius R_2 large. Some attempts were made to restart the model at level B, but without much success. The model became very sensitive to the values of various necessary parameters (such as the distance from level B to level A) and as the distance from B to C is much smaller than the distance from the nozzle to B, we should not expect the plume equations to apply very well in this region. Consequently it was decided to start the

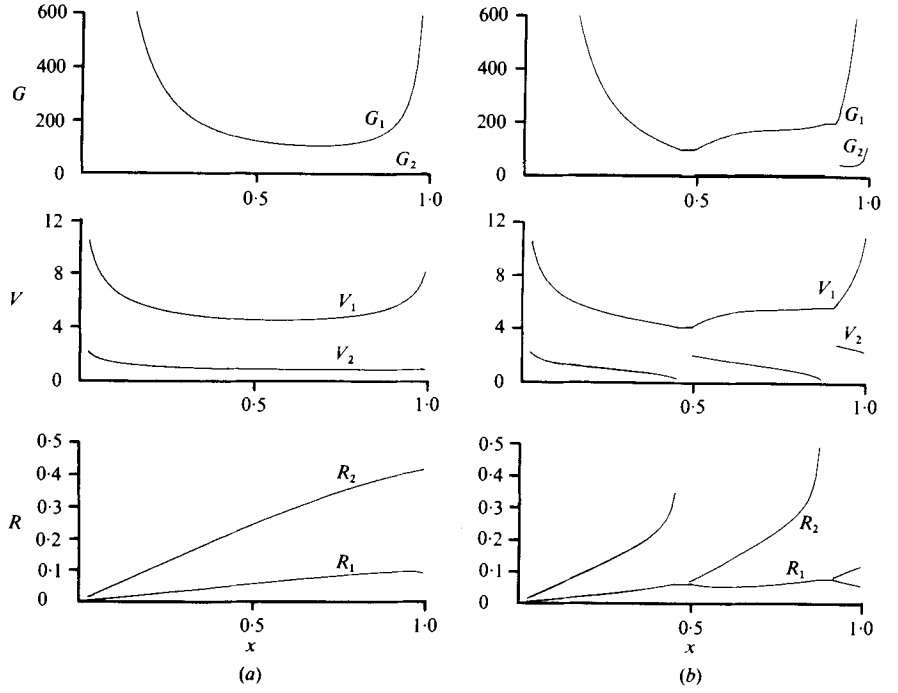

FIGURE 6. Graphs of velocities V, radii R and buoyancies G of the inner (subscript 1) and outer (subscript 2) plumes in the double-plume model for $M = 1$ with (*a*) $C = 0$ and (*b*) $C = 20$. Note that the spreading out of the outer plume occurs when its velocity goes to zero and its radius is large. Above this level, the outer plume starts again with $R_2 = R_1$. Note also the effects on the velocities and radii of the large accelerations caused by gas expansion at large x.

solutions at level C on figure 5, where the outer plume is assumed to have zero area ($R_2 = R_1$ at level C).

As levels A and C are close together, it seems reasonable to assume that the values of R_1, V_1 and G_1 at level C are the same as those at level A. Then we have the following equations to solve for V_2 and G_2 at level C:

$$d(S^2V_2)/dx = -\beta R_1 V_1 + R_1 V_2(1+\beta+\gamma), \tag{32}$$

$$d(S^2V_2^2)/dx = \beta R_1 V_2^2 - R_1 V_1 V_2(\beta-\gamma), \tag{33}$$

$$d(S^2V_2G_2)/dx = -\beta R_1 G_2(V_1-V_2) + \gamma R_1 V_2 G_{1L}. \tag{34}$$

The mass flux S^2V_2 is zero at this level, therefore $d(S^2V_2^2)/dx$ is simply $V_2\,d(S^2V_2)/dx$, and so (32) and (33) give

$$V_2 = \frac{\gamma}{1+\gamma} V_1 \quad \text{(at level } C\text{)}. \tag{35}$$

Similarly, from (32) and (34) we obtain

$$G_2 = -\frac{\gamma}{1+\gamma} G_{1L} \quad \text{(at level } C\text{)}. \tag{36}$$

These relations then enable the computer solutions to start again at level C.

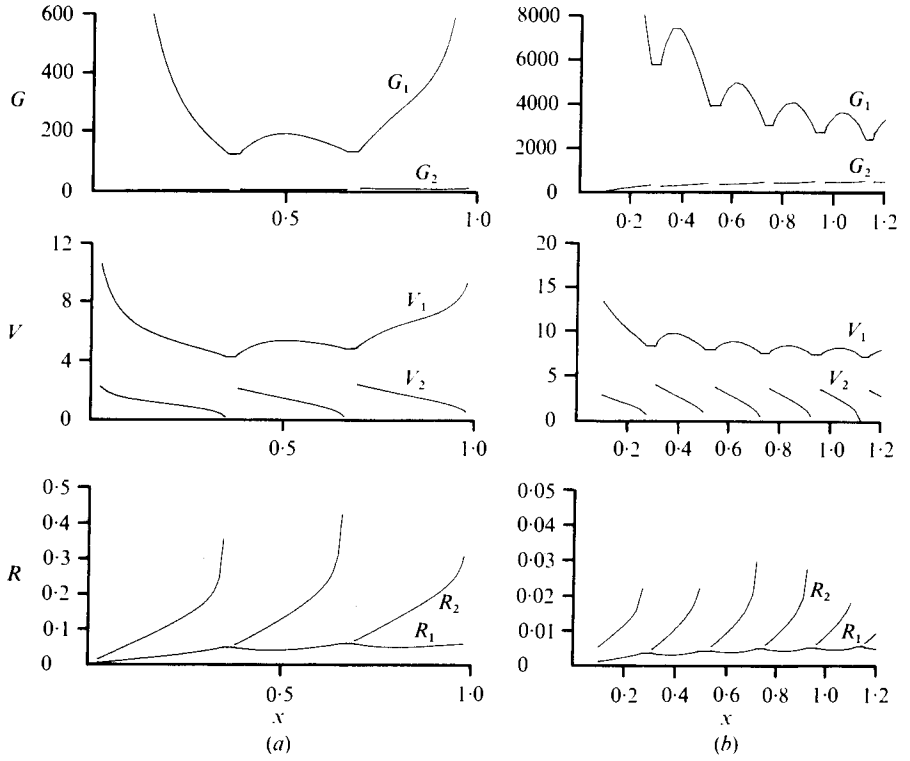

FIGURE 7. Graphs of velocities V, radii R and buoyancies G of the inner and outer plumes in the double-plume model for (*a*) $M = 1$, $C = 40$ and (*b*) $M = 0{\cdot}01$, $C = 30000$.

3.2.4. *Results of the double-plume model.* Several experiments were performed in the laboratory with $h = 1{\cdot}3$ m, the air flow rate Q_0 near 25 c.c./s (giving $M \doteqdot 0{\cdot}01$) and with values of the stratification parameter C between 7000 and 33000 (values of N^2 from 0·25 to 1·0 s^{-2}). These very high values of C had to be used because of the limitation on the depth of water in the experiments. (x at the surface is only 0·11.) At the lower end of this range of C only one spreading-out level was observed (see figure 3), while at the upper end of the range there were many spreading-out levels (see figure 4).

The values of β and γ were found by running the computer program for $M = 0{\cdot}01$ and $C = 30000$ with different values of β and γ and selecting the values which best reproduced the salient features of the experiments, namely the almost constant inner radius r_1 and inner velocity v_1. Values of $\beta = 0{\cdot}5 \pm 0{\cdot}1$ and $\gamma = 1{\cdot}0 \pm 0{\cdot}1$ achieved this, so $\beta = 0{\cdot}5$ and $\gamma = 1{\cdot}0$ were used for all calculations with the double-plume model in this paper. Perhaps this lower value of β may be associated with the smaller length scale of turbulent eddies in the inner plume, as compared with those in the outer plume, but an explanation of these values of β and γ lies beyond the scope of this paper.

Figure 6(*a*) shows graphs of the velocities, radii and buoyancies of both plumes for zero stratification and for $M = 1$. It is seen that the outer velocity is somewhat less than the inner velocity. The outer buoyancy G_2 is zero of course.

It should be noted that in each numerical solution in this paper the graphs finish at $x = 0{\cdot}985$. The value of x at any height z (m) for a nozzle depth h (m) is

$$x = z/H = z/(h + 10{\cdot}2),$$

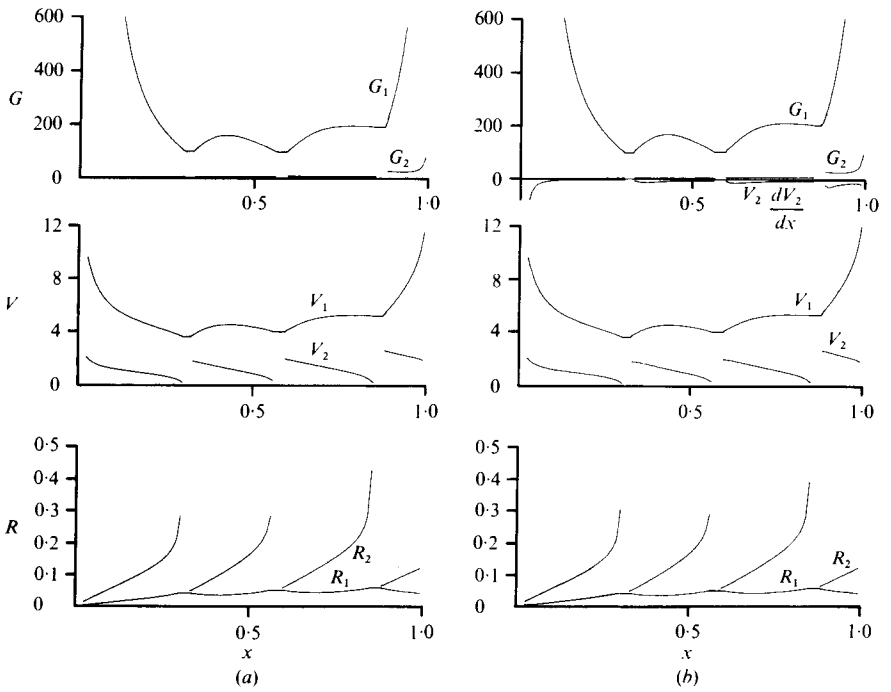

FIGURE 8. Graphs of velocities V, radii R and buoyancies G of the inner and outer plumes in the double-plume model for (*a*) $M = 0{\cdot}01$, $C = 40$ and (*b*) $M = 0{\cdot}01$, $C = 40$ and the body-force formulation described in appendix B.

so that if the water surface were to correspond to $x = 0{\cdot}985$ then the depth of the water would be given by $0{\cdot}985 = h/H = h/(h+10{\cdot}2)$, i.e. $h = 670\,\text{m}$. For nozzle depths less than this, the position of the surface will correspond to smaller values of x. For example, for a nozzle depth h of 10·2 m, the surface is at $x = 0{\cdot}5$, and for this nozzle depth values of $x > 0{\cdot}5$ have no physical meaning.

Figures 6 (*b*) and 7 (*a*) show the effect of increasing the stratification. The value which was arbitrarily chosen in all cases for the height from level A to level C in figure 5 was $0{\cdot}4 \times R_1$ (near A). It can be seen from these figures that, as the stratification increases, the number of times that the fluid spreads out is increased and the distance between the levels at which it does this is decreased.

The influence of the source strength parameter M on the non-dimensional solutions can be seen by comparing figures 7 (*a*) and 8 (*a*). The lower value of M means that in the non-dimensional solutions the plume effectively has less buoyancy (because the slip velocity of the bubbles is now a larger proportion of the plume velocity) and so it spreads out more rapidly.

The experiments were carried out in a tank of small horizontal extent and hence the stratification of the 'environment' in the tank changed appreciably during the course of an experiment. Consequently, it was possible to get meaningful results for only about the first minute of operation. This also means that the unsteady effects produced by starting the plume are more pronounced than one would like in an experiment which is trying to model a steady-state situation. The experimental restriction on the depth of the water, which necessitates high values of C, implies that the distance

between successive settling-out heights is not much larger than the inner radius r_1. (This similarity of scales can be seen in figure 4, although since the bubbles are not visible in these shadowgraphs only the edge of the outer plume can be seen.) For this reason we should not expect the assumptions involved in deriving the model to be an accurate representation of the experiments.

The limitations on both the depth and the horizontal area of the tank preclude any detailed quantitative test of the model, but the main features of the experiments, namely the narrow inner plume and the successive levels of spreading out, are reproduced well. For example, in the case $M = 0{\cdot}01$, $C = 30000$, figure 7(*b*) shows that the average x spacing between the spreading-out levels is about 0·019, which for the experiment of figure 4 corresponds to a difference in height of 22 cm. From the groups of ten 1 cm markings on the tank in figure 4, this can be seen to be in reasonable agreement with experiment.

Returning to the oil-well blow-out problem, Topham (1974) suggests values of $Q_0 (\sim 0{\cdot}5\,\mathrm{m^3/s})$ and h (20–200 m) which give $M \approx 1$. Taking an average value of N^2 of 10^{-4} from Hunkins (1974) as being typical for the 200 m case, we obtain $C \approx 50$. These values of M and C are certainly in the range where we expect spreading out to occur (cf. figure 7*a*). If the droplets of oil in the plume remain fairly large (i.e. if an emulsion does not occur) then we can imagine that even when the oil has spread out horizontally it will still eventually find its way to the surface within a few hours. However the formation of an emulsion seems likely (Chen 1974; Topham 1974), depending on the exact chemical composition of the oil and the nature of the turbulence close to the blow-out, and in this situation the oil could spend many days in the ocean and be carried far afield by slow currents.

It is a pleasure to acknowledge the many stimulating dicussions I have had with Professor J. S. Turner, and to thank Dr P. F. Linden for his many helpful comments on an earlier draft of this paper.

Appendix A. Power-series solution for the double-plume model

On substituting the truncated power series of § 3.2.2 into (28)–(31), we obtain the following cubic for r_1:

$$r_1^3 + a_2 r_1^2 + a_1 r_1 + a_0 = 0, \tag{A 1}$$

where

$$a_2 = E^{-1}(-\tfrac{5}{4}\beta(1-\tfrac{5}{6}\gamma^2) - \tfrac{25}{6}\gamma^3),$$

$$a_1 = E^{-1}(-\tfrac{1}{4}\beta^2 - \tfrac{5}{4}\gamma^2 - \tfrac{25}{16}\gamma^4),$$

$$a_0 = E^{-1}(\tfrac{3}{4}\gamma^2\beta),$$

and

$$E = \tfrac{25}{9}[1-(\gamma-\tfrac{1}{4}\beta)^2].$$

It can be shown that for $E > 0$ (and of course $\gamma > 0$ and $\beta > 0$) the only physically allowable solution of (A 1) will have $q^3 + p^2 < 0$, where

$$q = \tfrac{1}{3}a_1 - \tfrac{1}{9}a_2^2 \quad \text{and} \quad p = \tfrac{1}{6}(a_1 a_2 - 3a_0) - \tfrac{1}{27}a_2^3.$$

This solution is

$$r_1 = -(-q)^{\frac{1}{2}}\cos\tfrac{1}{3}\theta - \tfrac{1}{3}a_2 + (-3q)^{\frac{1}{2}}\sin\tfrac{1}{3}\theta,$$

where

$$\theta = \tan^{-1}\{(-q^3-p^2)^{\frac{1}{2}}/p\}, \quad -\tfrac{1}{2}\pi < \theta \leqslant \tfrac{1}{2}\pi.$$

For $E < 0$, q^3+p^2 can be of either sign. When $q^3+p^2 < 0$, the required solution is

$$r_1 = 2(-q)^{\frac{1}{2}} \cos \tfrac{1}{3}\theta - \tfrac{1}{3}a_2$$

and when $q^3+p^2 > 0$

$$r_1 = [p+(q^3+p^2)^{\frac{1}{2}}]^{\frac{1}{3}} + [p-(q^3+p^2)^{\frac{1}{2}}]^{\frac{1}{3}} - \tfrac{1}{3}a_2.$$

v_1, d_1 and b_1 can be found in terms of r_1 from the following expressions:

$$v_1 = \left[\tfrac{4}{3}r_1^2 + \frac{\gamma-\beta}{\gamma+\beta}(\beta-\tfrac{5}{3}r_1)r_1 + \frac{\beta r_1(\beta-\frac{5}{3}r_1)^2}{(\gamma+\beta)^2}\right]^{-\frac{1}{3}},$$

$$d_1 = v_1(\beta-\tfrac{5}{3}r_1)/(\gamma+\beta),$$

$$b_1 = [\tfrac{3}{4}\beta r_1 + \tfrac{3}{4}(\gamma-\beta)r_1 v_1/d_1]^{\frac{1}{2}}.$$

Proceeding to the next terms in the series, we obtain four simultaneous linear equations in the four unknowns. These are expressed in the matrix form given below and the solutions for r_2, v_2, b_2 and d_2 can be readily obtained by standard matrix methods. We set

$$\begin{bmatrix} c_{11} & c_{12} & c_{13} & c_{14} \\ c_{21} & c_{22} & c_{23} & c_{24} \\ c_{31} & c_{32} & c_{33} & c_{34} \\ c_{41} & c_{42} & c_{43} & c_{44} \end{bmatrix} \begin{bmatrix} r_2 \\ v_2 \\ b_2 \\ d_2 \end{bmatrix} = \begin{bmatrix} 0 \\ 0 \\ 0 \\ -M^{-\frac{1}{3}}v_1^{-1} \end{bmatrix},$$

where

$$c_{11} = \tfrac{7}{3}v_1, \quad c_{12} = 2r_1-\beta, \quad c_{13} = 0, \quad c_{14} = \gamma+\beta,$$

$$c_{21} = -\beta d_1 - (\gamma-\beta)v_1, \quad c_{22} = -(\gamma-\beta)r_1, \quad c_{23} = \tfrac{10}{3}b_1 d_1, \quad c_{24} = \tfrac{14}{3}b_1^2 - 3\beta r_1,$$

$$c_{31} = 2r_1 d_1^2 - \beta v_1 S + (\gamma+\beta)d_1 S, \quad c_{32} = -\beta r_1 S, \quad c_{33} = 2b_1 d_1^2 - 4b_1 d_1 S,$$

$$c_{34} = 2d_1(b_1^2+r_1^2) - 2b_1^2 S + (\gamma+\beta)r_1 S,$$

$$c_{41} = \tfrac{10}{3}r_1 v_1^3 + (\gamma-\beta)d_1 v_1^2 + \beta d_1^2 v_1, \quad c_{42} = \tfrac{10}{3}r_1^2 v_1^2 + (\gamma-\beta)r_1 d_1 v_1 + v_1^{-1},$$

$$c_{43} = 0, \quad c_{44} = (\gamma-\beta)r_1 v_1^2 + 2\beta r_1 v_1 d_1,$$

$$S = \tfrac{10}{3}(b_1^2 d_1 + r_1^2 v_1).$$

Appendix B. Some thoughts on the body forces in a double-plume model

It is not obvious how to account for the body forces acting on the inner and outer plumes. The assumption that pressure surfaces remain horizontal across the environment and both plumes leads to equations (15) and (16) for the conservation of momentum flux. Berson & Baird (1975) postulated a model for cumulonimbus convection which involves a plume element surrounded by other elements, two of which have different densities to the plume element in question. They took the body force to be given by a weighted sum of locally defined buoyancy forces, namely

$$g \sum_i A_{i\pm1} \frac{\rho_{i\pm1}-\rho_i}{\rho_{i\pm1}},$$

where the weighting factors $A_{i\pm1}$ are the ratio of the length of contact between fluid i and fluid $i \pm 1$ to the total perimeter of the plume element i. This method of weighting of the relative buoyancy terms with the relevant proportion of the periphery of the plume element seems to have no clear physical justification.

If we are to pursue the argument of referring buoyancy to the local elements, then

this must be done in a frame of reference which is fixed to these surrounding elements (i.e. an accelerating frame of reference). This implies that the non-dimensional momentum equation for the inner plume becomes

$$d(R_1^2 V_1^2)/dx = R_1^2(G_1 + G_2 + V_2\, dV_2/dx) + \beta R_1 V_2(V_1 - V_2) - \gamma R_1 V_1 |V_2| \qquad \text{(B 1)}$$

instead of (23). ($V_2\, dV_2/dx$ is the non-dimensional acceleration of the outer plume.)

Now in order to obtain the momentum equation for the outer plume, it seems reasonable to assume that the overall momentum equation, taken across both plumes, should still apply, i.e.

$$d(R_1^2 V_1^2 + S^2 V_2^2)/dx = R_1^2 G_1 - S^2 G_2. \qquad \text{(B 2)}$$

This averaging across both plumes is analogous to what is done for a single plume when Gaussian profiles are assumed, except perhaps that now we expect a rather sharp change in velocity and buoyancy between the two plumes. Subtracting (B 1) from (B 2), we obtain

$$d(S^2 V_2^2)/dx = -S^2 G_2 - R_1^2(G_2 + V_2\, dV_2/dx) - \beta R_1 V_2(V_1 - V_2) + \gamma R_1 V_1 |V_2|. \qquad \text{(B 3)}$$

In our application to bubble plumes, G_1 will normally be significantly larger than both G_2 and $V_2\, dV_2/dx$, and also since G_2 will always be positive and $V_2\, dV_2/dx$ negative (except for large x), we conclude [by inspection of (B 1)] that this different formulation of the momentum equations is likely to have little effect on the motion of the inner plume. What will its effect be on the outer plume? When $S^2 \gg R_1^2$ the first term on the right-hand side of (B 3) will dominate the second term, but when $S^2 \ll R_1^2$ the second term can be more important than the first. However, for these small values of S^2, the velocity V_2 is not small and the mixing term $R_1 V_2^2$ is larger than both of the first two terms.

For these reasons we should not expect the solutions to be changed very much owing to this reformulation of the body forces and indeed all the numerical examples which were done confirmed this expectation. All the computer graphs were virtually identical to their counterparts described in § 3.2.4. Figure 8(*b*) shows the solutions obtained using these new equations for $M = 0{\cdot}01$ and $C = 40$, and is to be compared with figure 8(*a*).

Although it has been shown that this reformulation of the body forces does not significantly affect the results of a bubble plume model, it is expected to be important for other double-plume structures (e.g. atmospheric convection) where G_1 is not much larger than G_2.

REFERENCES

Baines, W. D. 1961 The principles of operation of bubbling systems. *Proc. Symp. Air Bubbling, Ottawa.*

Berson, F. A. & Baird, G. 1975 A numerical model of cumulonimbus convection generating a protected core. *Quart. J. Roy. Met. Soc.* **101**, 911–928.

Bulson, P. S. 1968 The theory and design of bubble breakwaters. *Proc. 11th Conf. Coastal Engng, London*, p. 995.

Chen, E. C. 1974 Stability of crude oil-in-water emulsions. *J. Can. Pet.*, Jan–March 1974, pp. 38–41.

Ditmars, J. D. & Cederwall, K. 1974 Analysis of air-bubble plumes. *Proc. 14th Conf. Coastal Engng, Copenhagen*, p. 2209.

Hoult, D. P. 1969 *Oil on the Sea.* Plenum.

Hunkins, K. H. 1974 Subsurface eddies in the arctic ocean. *AIDJEX Bull.* no. 23, pp. 9–36.

JONES, W. T. 1972 Air barriers as oil-spill containment devices. *J. Soc. Pet. Engng*, pp. 126–142.

KOBUS, H. E. 1968 Analysis of the flow induced by air-bubble systems. *Proc. 11th Conf. Coastal Engng, London*, pp. 1016–1031.

MARKS, C. H. & CARGO, D. G. 1974 Field tests of a bubble screen sea nettle barrier. *J. Mar. Tech.* pp. 33–39.

MORTON, B. R. 1962 Coaxial turbulent jets. *Int. J. Heat Mass Transfer* **5**, 955–965.

MORTON, B. R., TAYLOR, G. I. & TURNER, J. S. 1956 Turbulent gravitational convection from maintained and instantaneous sources. *Proc. Roy. Soc.* A **234**, 1–23.

TAYLOR, G. I. 1955 The action of a surface current used as a breakwater. *Proc. Roy. Soc.* A **231**, 466–478.

TOPHAM, D. R. 1974 The hydrodynamic aspects of the behaviour of oil released under sea ice. *Int. Rep. Dept. Electrical Engng, Univ. Alberta.*

TURNER, J. S. 1963 The motion of buoyant elements in turbulent surroundings. *J. Fluid Mech.* **16**, 1–16.

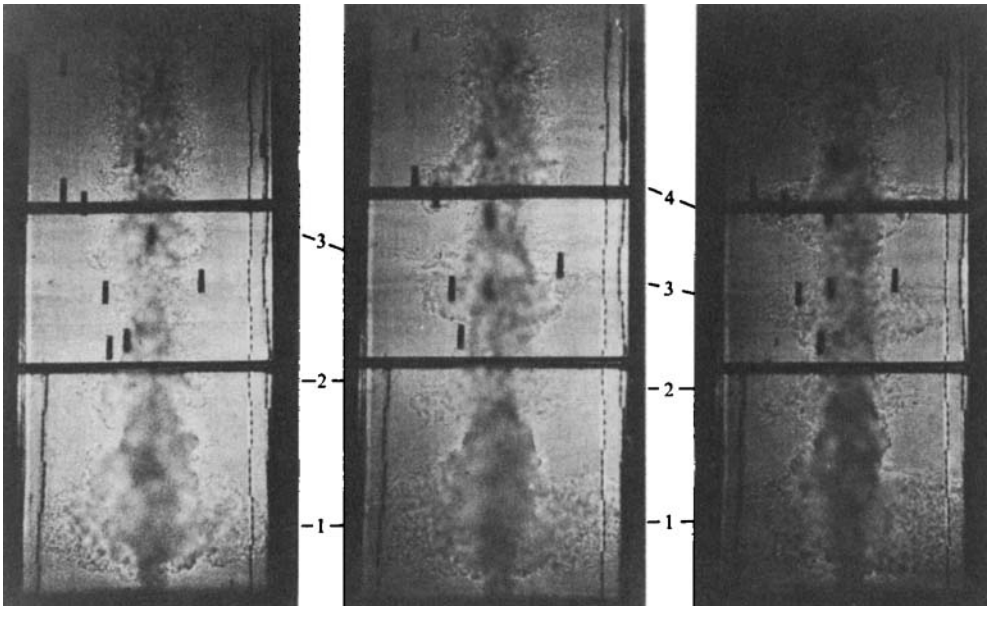

FIGURE 4. Three shadowgraphs taken at successive times (from left to right) during the course of an experiment with $M = 0{\cdot}01$, $C = 30000$. The spreading-out stages are numbered from the nozzle upwards. The small cylinders are the coloured density-marker bottles.